Magnetic Field Penetration Into a Conducting Hohlraum

Alec Kirkley
Pittsford Sutherland High School
Pittsford, NY
Advisor: Dr. Gennady Fiksel

Laboratory for Laser Energetics
University of Rochester
Rochester, NY
September 2012

Abstract

A gold hohlraum will be used for a variety of MIFEDS (Magneto-Inertial Fusion Electrical Discharge System) experiments on the Omega laser system at the Laboratory for Laser Energetics (LLE) of the University of Rochester, NY, and the magnetic field penetration into the hohlraum is of interest. The dynamics of the axial magnetic field penetration into the conductive hohlraum was analyzed theoretically, and a small-scale tabletop experiment was designed to test the predictions. The experiment used a solenoid to generate a magnetic field, which was measured by a multi-turn B-dot probe. For this experiment, the hohlraum was substituted with thin-wall copper tubing with a diameter of 2.54 cm. Three different lengths of tube (2.54 cm, 5.08 cm, and 7.62 cm) were used to measure the attenuation and phase shift of the magnetic field inside the tubing in comparison with the outside. The measured attenuation and phase shift results are consistent with theoretical predictions, and the results are directly applicable to the field attenuation in an actual hohlraum.

1. Introduction

Two light atomic nuclei can combine to create immense quantities of energy in a process called nuclear fusion. The advantage of nuclear fusion over other methods of harnessing energy is that fusion is sustainable and safe for the environment. Nuclear fusion research is being conducted around the world due to its potential for energy production, and the Laboratory for Laser Energetics (LLE) is one major contributor to this research. Inertial confinement fusion is the main topic of interest at LLE, where a cryogenic target is heated and compressed by the Omega laser system.

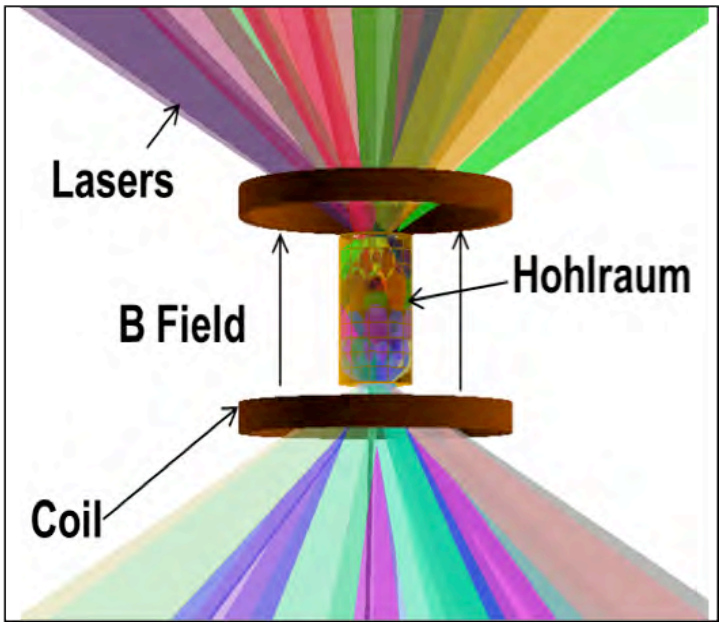

Figure 1. Hohlraum Diagram: A target plasma is confined in a hohlraum by an applied magnetic field during magneto-inertial fusion.

A strong pulse of magnetic field could be used to improve plasma confinement in an inertial confinement fusion (ICF) implosion. The Magneto-Inertial Fusion Electrical Discharge System (MIFEDS)[(1)] is used to create this magnetic field, which can confine the fusion fuel as it is heated into the plasma state.[(2)] In the process of magneto-inertial fusion, the magnetic field provided by MIFEDS helps reduce the loss of thermal energy, while containing the plasma and allowing it to be heated by inertial compression.

One experiment planned for the Omega laser system using MIFEDS has a goal of studying the effect of a magnetic field on the confinement and transport of fast electrons in a hohlraum plasma. Hohlraum plasma fusion (Fig. 1) is an ICF concept wherein a spherical fusion

target placed inside a thin-wall high-Z metal cylinder is compressed by intense x-ray radiation resulting from the interaction of powerful laser radiation with the inner walls of the hohlraum. This concept is called “indirect drive” to distinguish it from the “direct drive” concept wherein a fusion target is directly compressed by laser radiation. One of the by-products of the laser-wall interaction in a hohlraum is the production of energetic electrons that can penetrate into the target and adversely affect its compression and heating. A magnetic field can potentially isolate the target from the fast electrons, which is the main motivation behind the planned experiment. It is essential that the magnetic field produced by MIFEDS is strong and can penetrate into the hohlraum.

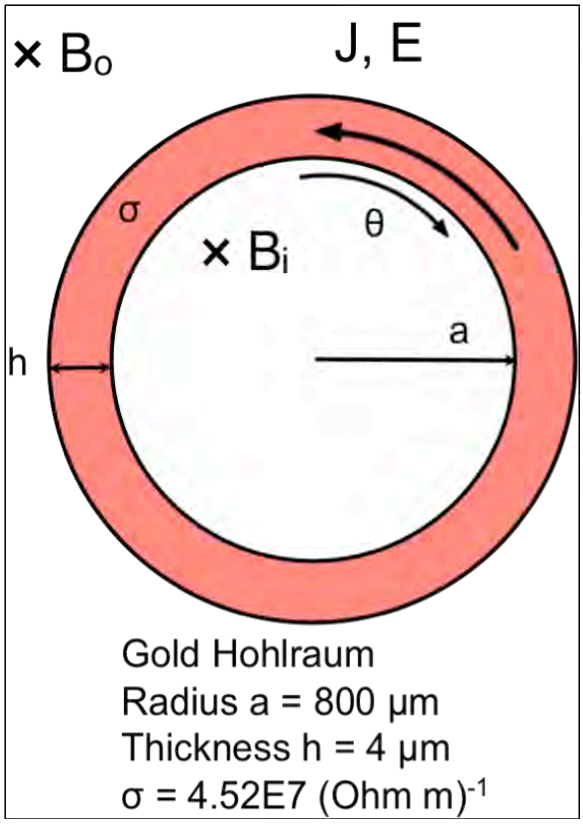

Figure 2. Cross Section of a Hohlraum in an Applied External Field: B_0 is the external magnetic field, J is the induced shell current density, E is the induced electric field, and B_i is the internal attenuated magnetic field. Dimensions for the hohlraum are given. The hohlraum length is 2.4 mm. Note that the current and electric field are in the negative θ direction.

However, because the hohlraums are made out of conductive metal, they can partially screen and attenuate the externally applied pulsed magnetic field. The project described in this report was designed to investigate and quantify this effect. The purpose of this project is two-pronged. First, we wanted to understand the mechanism and dynamics of magnetic field penetration so we can predict the field attenuation and the time it takes the magnetic field to penetrate into the

interior of the hohlraum. Second, a table-top-scaled experiment was built to test our predictions. In the future, the magnetic field penetration will be studied using a real hohlraum.

2. Mathematical Modeling

2.1 Background

When an axial external magnetic field B_0 is applied to a conductive cylindrical shell, it induces a poloidal current J that runs around the shell (see Fig. 2, which also shows the hohlraum dimensions). The current, in turn, generates a magnetic field opposite to the applied magnetic field, so that the field inside the shell B_i is initially zero. Initially, the current J is concentrated in a thin skin layer on the outside of the cylinder. Later, the skin layer expands to the thickness of the shell and eventually starts decaying so the internal field B_i starts to grow. Overall, the internal field is attenuated and delayed with respect to B_0. The goal of the model is to describe this process. Two characteristic time scales need to be investigated regarding this attenuation, namely the time for current to equilibrate across the shell due to the skin effect, and the resistive current decay time in the shell. A mathematical relationship between the inner and outer fields is desired in order to predict the field attenuation.

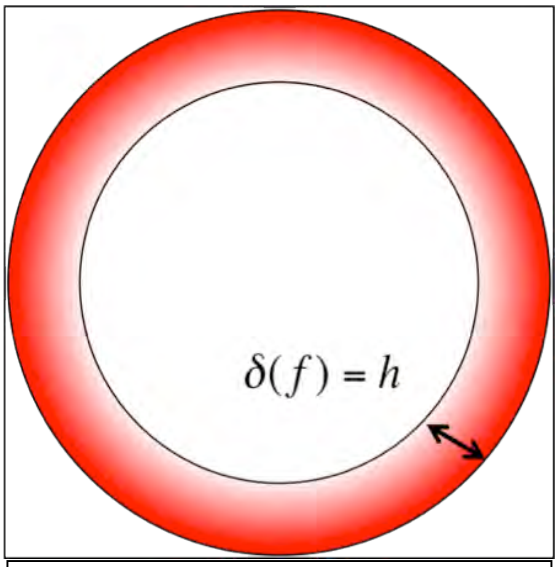

Figure 3. Skin Depth of Hohlraum Shell: The intensity of the red shading indicates J, the current density, which decreases as distance from the surface increases. In this figure the skin depth at frequency *f*, $\delta(f)$, equals the shell thickness h.

2.2 Skin Time

The physics associated with magnetic field penetration can be investigated by considering imposed magnetic fields B_0 that oscillate sinusoidally with a frequency f. When current is introduced to a conductive shell, the skin effect causes it to initially concentrate near the surface. As the current density gets distributed through the conductor, it decreases exponentially as a function of depth from the surface. At the skin depth, which depends on f, the current has reached 1/e of its initial surface value.(3) Figure 3 shows the hohlraum shell, with the decreasing current density across it. The skin depth δ can be shown to be:

$$\delta = \sqrt{\frac{1}{\mu_0 \sigma \pi f}}, \tag{1}$$

where μ_o is the magnetic constant and σ is the conductivity of the cylinder. When the skin depth is greater than the shell thickness h, it can be assumed that the current has essentially equilibrated across the shell. The frequency f_h at which the skin depth equals the shell thickness h can therefore be used as a figure of merit. For frequencies lower than f_h the current across the shell can be considered uniform. The skin time T_{skin} is defined as $1/f_h$. From Eq. 1,

$$T_{skin} = \mu_0 \pi \sigma h^2 \tag{2}$$

For a gold hohlraum with dimensions as in Fig. 2, f_h =349 MHz, and its inverse, the time for the current to penetrate the shell T_{skin} is 2.9 ns. This is very small compared with the rise time of MIFEDS (600 μs) so the current can be assumed uniform within the shell.

2.3 Resistive Current Decay Time

Under the assumption of uniform current distribution across the shell, the electric and magnetic fields can be calculated using Faraday's Law (Eq. 3), Ohm's Law (Eq. 4), and Ampere's Law (Eq. 5):

$$2\pi a E_\theta = \frac{-d\Phi}{dt} \tag{3}$$

$$E_\theta = \frac{J_\theta}{\sigma} \tag{4}$$

$$\oint B \bullet dl = \mu_0 I \tag{5}$$

where a is the hohlraum radius, E_θ (= -E) is the electric field, J_θ (= -J) is the current density, l is a length element on a rectangular loop in the (r,z) plane of height h connecting the two surfaces, I is the current through this loop, and Φ (= $B_i \pi a^2$) is the magnetic flux across the cylinder's cross section. The magnetic field is in the z direction and into the page in Fig. 2. E_θ and J_θ are defined in the θ direction, which is in the clockwise direction with repect to the magnetic field. Algebraic manipulation yields the following expressions for the electric and magnetic fields:

$$\begin{aligned} E_\theta &= \frac{-a}{2}\frac{dB_i}{dt} \\ &= \frac{J_\theta}{\sigma} \\ &= \frac{B_i - B_0}{\mu_0 \sigma h} \end{aligned} \tag{6}$$

Combining the first and third terms and isolating B_o gives a differential equation that relates the inner and outer magnetic fields:[4]

$$B_0 = B_i + \tau \frac{dB_i}{dt} \tag{7}$$

where τ is a time constant given by:

$$\tau = \frac{\mu_0 \sigma a h}{2} \tag{8}$$

In the case where B_o is suddenly applied to the outside of the hohlraum with $B_i = 0$ when t = 0, Eq. 7 can be integrated to give

$$B_i(t) = B_0(1 - e^{-t/\tau}) \tag{9}$$

so that B_i(t) approaches B_0 for times greater than τ. As this happens, J approaches 0 from Eq. 6. For this reason τ is known as the resistive current decay time.

2.4 Response to a Sinusoidal Magnetic Field

Information on the resistive current decay time can be attained by imposing a sinusoidal external magnetic field. This results in a sinusoidal shell current and internal B field:

$$B_0(t) = B_0 e^{i\omega t} \tag{10}$$

$$B_i(t) = A e^{i\omega t} \tag{11}$$

where A is the complex amplitude of B_i and ω (=2πf) is the angular frequency of the B fields. Solving for A by substituting into Eq. 7:

$$A = \frac{B_0}{1 + i\omega\tau} \tag{12}$$

an expression for a sinusoidal B_i results:

$$B_i(t) = \frac{B_0}{1 + i\omega\tau} e^{i\omega t} \tag{13}$$

Finding the absolute value of the amplitude of B_i yields:

$$\left|B_i\right| = \frac{\left|B_0\right|}{\left|1 + i\omega\tau\right|} = \frac{B_0}{\sqrt{1 + \omega^2\tau^2}} \tag{14}$$

The field attenuation can be defined as:

$$Attenuation = \frac{\left|B_i\right|}{\left|B_0\right|} = \frac{1}{\sqrt{1 + \omega^2\tau^2}} \tag{15}$$

Taking the inverse tangent of the imaginary component of B_i over the real component of B_i yields an expression for the phase shift (delay) of B_i relative to B_o:

$$\varphi = \tan^{-1}(-\omega\tau) \tag{16}$$

Eqs. 15 and 16 reveal that both the attenuation and phase shift depend on the single dimensionless parameter $\omega\tau$ where τ, given by Eq. 8, contains the important hohlraum characteristics such as dimensions and conductivity. In this sense, the model should accurately describe the dynamics of magnetic field penetration in the real hohlraum as well as in any conductive cylinder. Therefore, in order to test the accuracy of Eqs. 7, 15 and 16, we designed and built a simple tabletop experiment substituting a hohlraum with a copper cylinder. If the predictions (15) and (16) were proven true, then the model could be applied to the real hohlraum.

3. Experimental Design

3.1 Tabletop Experiment

Originally, in order to test the theoretical predictions for field attenuation (Eq. 15) and phase shift (Eq. 16), the hohlraum was to be placed in a sinusoidal axial field, and the experimental results measured with a Faraday probe were to be compared with predictions. The

hohlraum had not yet been manufactured, so in order to test the theory, a tabletop experiment (Figs. 4 and 5) was designed to test the attenuation and phase shift into copper tubing, which behaves consistently with the same physics. Predictions (Eq. 15, Eq. 16) were derived for an infinite length cylinder, so three copper tubes of different lengths were tested to see if the results became more consistent with predictions as the tube size increased. In order to provide an axial sinusoidal magnetic field inside the tubing, a solenoid was constructed out of copper wire, and was connected to a 1.3 ohm resistor in series with a sinusoidal function generator as the voltage source. The voltage across the resistor was measured with an oscilloscope to determine the electrical current in the solenoid. The field inside the tubing was measured with a B-dot probe, which was a smaller solenoid also

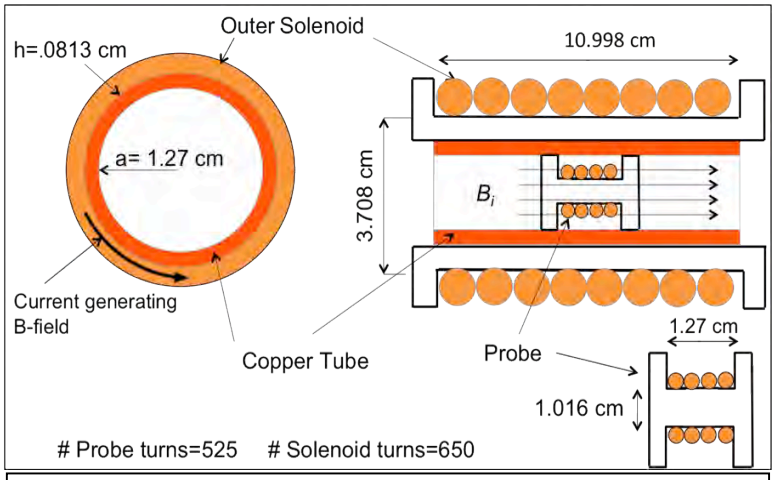

Figure 4. Experimental Diagram: An axial, sinusoidal magnetic field generated by the outer solenoid penetrates through the copper tube. The inner field B_i is measured by a B-dot probe. Shown are front and side views of the outer solenoid surrounding the copper tubing where the B-dot probe is placed.

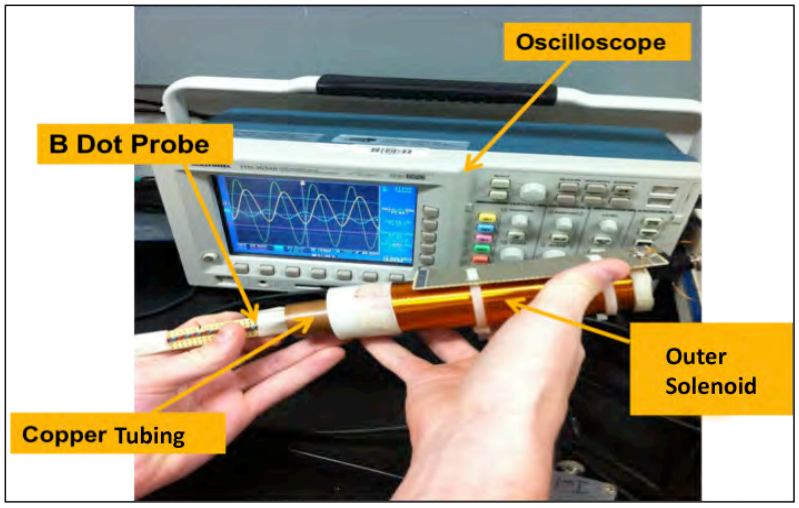

Figure 5. Experimental Set Up: The tabletop experiment was simple and inexpensive, but still involved the same physics as the hohlraum experiment would have.

constructed out of copper wire. The voltage across the B-dot probe was measured to determine the field inside the tubing. The measurements were taken with variable function generator frequencies in the range from 20 Hz to 4000 Hz. The attenuation and phase shift were measured as functions of the generator frequency for each size of copper tubing. Figure 6 is a graph of the expected inner and outer magnetic fields for the copper at a mid-range frequency. The inner magnetic field lags behind the outer magnetic field by a phase shift τ.

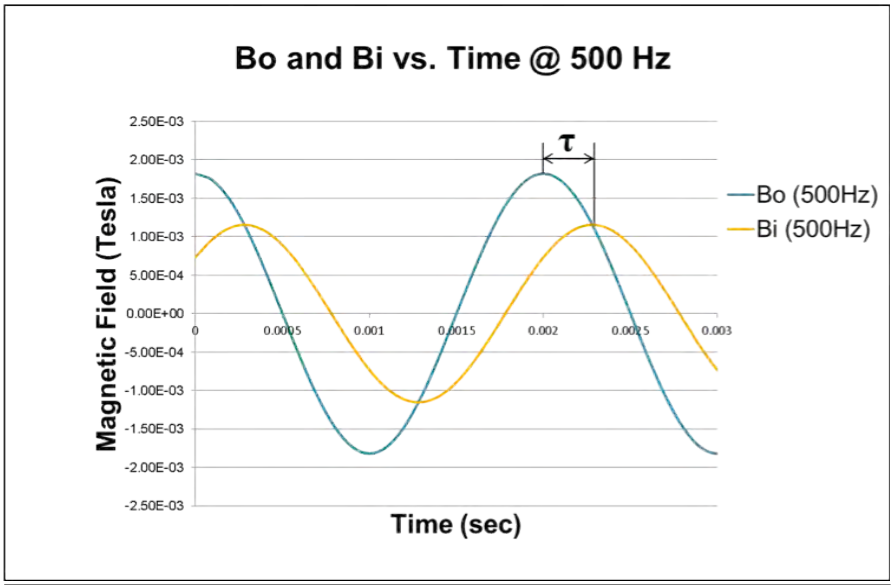

Figure 6. Modeled B_i and B_0: The inner and outer fields were modeled for an infinitely long copper tube of otherwise the same dimensions as the tubes that were tested. Shown is the modeling for an intermediate frequency.

3.2 Data Analysis

The field generated by the outer solenoid is given by:

$$B_0 = \mu_0 \frac{N_s}{l_s} I_s = \mu_0 \frac{N_s}{l_s} \frac{V_R}{R} \tag{17}$$

where I_s is the outer solenoid current, N_s is the number of turns of wire in the solenoid, l_s is the length of the solenoid, R is the 1.3 ohm resistor, and V_R is the measured resistor voltage. The field inside the tubing can be evaluated from the B-dot probe measurement:

$$V_p = \pi r_p^{\,2} N_p \frac{dB_i}{dt} \tag{18}$$

where V_p is the measured probe voltage, r_p is the probe radius, and N_p is the number of probe turns. Solving for the time derivative of B_i:

$$\frac{d}{dt}(B_i(t)) = \frac{d}{dt}(B_i e^{i\omega t}) = i\omega B_i(t) \tag{19}$$

Eqs. 18 and 19 can be algebraically manipulated to derive an expression for the experimental field attenuation:

$$\frac{|B_i|}{|B_0|} = \left(\frac{V_p}{V_R}\right)\left(\frac{l_s R}{\pi r_p^{\,2} N_p \mu_0 N_s \omega}\right) \tag{20}$$

4. Results

4.1 Attenuation Results

Figure 7 is a graph of the expected attenuation and the recorded attenuations versus the applied frequency. The experimental attenuation results were consistent with the predictions, as it appears that the graphs for increasing tube

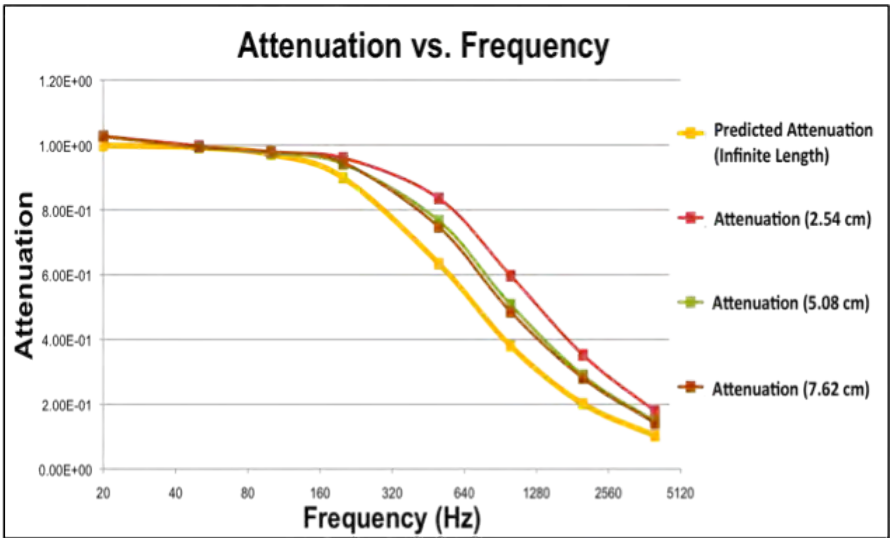

Figure 7. Experimental Attenuation as a Function of Frequency: As the tube size increases, the attenuation results appear to approach the theoretical values for an infinite copper tube length.

lengths approach the theoretical attenuation graph for an infinite tube length.

4.2 Phase Shift Results

Figure 8 shows the expected and recorded phase shifts graphed against the applied frequency. The experimental phase shift results were consistent with the predictions, as it appears that the graphs for increasing tube lengths approach the theoretical graph for an infinite tube length, as with Fig. 7.

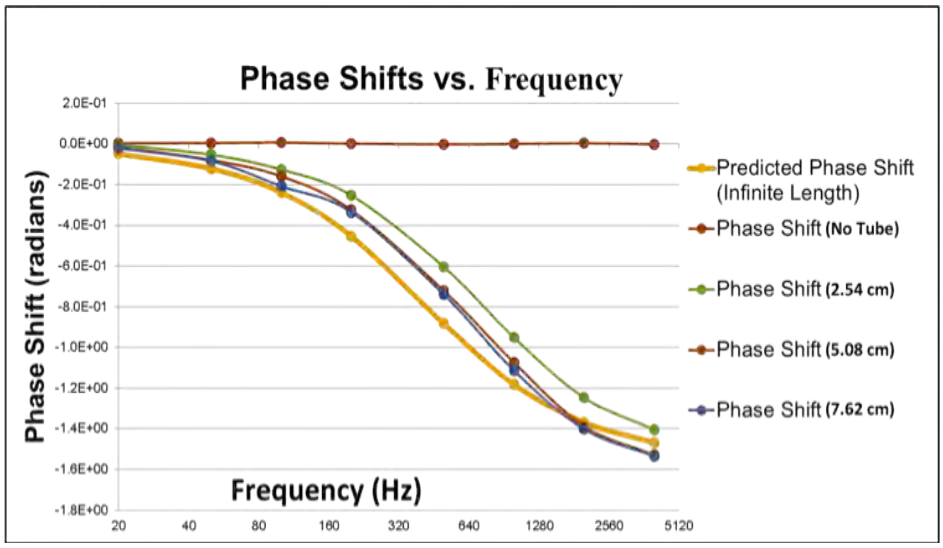

Figure 8. Experimental Phase Shifts as a Function of Frequency: As the tube size increases, the phase shift results appear to approach the theoretical values for an infinitely long copper tube.

4.3 Possible Experimental Error

While all the experimental results were close to the predictions, some small differences are observed. One possible explanation is the effect of a finite wall thickess of the copper tubing. This could cause a smaller magnetic field inside the tube and a greater phase shift at higher frequencies. Also, the conductivity of the copper used may not have actually been exactly the same as the value used for predictions.

5. Conclusions

The magnetic field penetration into a hohlraum was modeled analytically and tested using a tabletop experiment with copper tubing. A differential equation relating an axial external magnetic field and the resulting attenuated internal magnetic field was developed as well as an

expression for a delay time constant between the fields. The resistive decay time for the shell current was found to be the main source of attenuation, and the skin time was found to be insignificant at low frequencies. The tabletop experiment involved the use of three different lengths of copper tubing, since an actual hohlraum was not available, and the phase shift and attenuation results were consistent with mathematical predictions. This physics can now be applied to the real hohlraum.

An attenuation close to 1.0 is predicted for the actual hohlraum, meaning that the magnetic field penetrates into the interior of the hohlraum. Future testing will be done on a hohlraum with a Faraday probe to measure the attenuation and phase shift. Knowing that a magnetic field can successfully penetrate the hohlraum is essential to MIFEDS experiments, so that the fusion plasma can be properly contained to reduce thermal losses.

Acknowledgements

I thank Dr. Gennady Fiksel for his assistance and guidance during this project, Daniel Barnak and Po-Yu Chang for their teaching and help with the assembling of the experiment, and Dr. Craxton for giving me the opportunity to participate in this research.

References

1. Gotchev et al., "Seeding Magnetic Fields for Laser-Driven Flux Compression in High-Energy-Density Plasmas," Review of Scientific Instruments, **80**, 043504 (2009).
2. Gotchev et al., "Laser-Driven Magnetic-Flux Compression in High-Energy-Density Plasmas, Physical Review Letters, **103**, 215004 (2009).
3. W.N Cottingham and D.A. Greenwood, "Electricity and Magnetism," Cambridge University Press, 1991.
4. Gennady Fiksel, "B-Field Penetration Powerpoint", 2012.